Bacillus subtilis remains translationally active after CRISPRi-mediated replication initiation arrest

Vanessa Muñoz-Gutierrez[1,2], Fabián A. Cornejo[1], Katja Schmidt[1], Christian K. Frese[1], Manuel Halte[3], Marc Erhardt[1,3], Alexander K.W. Elsholz[1], Kürşad Turgay[1,2*], Emmanuelle Charpentier[1,4]

[1]Max Planck Unit for the Science of Pathogens, D-10117 Berlin, Germany

[2]Institute of Microbiology, Leibniz Universität Hannover, D-30419 Hannover, Germany

[3]Humboldt-Universität zu Berlin, Institute for Biology – Bacterial Physiology, Philippstr. 13, D-10115 Berlin, Germany

[4]Institute for Biology, Humboldt-Universität zu Berlin, D-10115 Berlin, Germany

[*]Corresponding author

Keywords:

Bacillus subtilis, replication, *oriC*, DnaA boxes, CRISPRi

Correspondence:

Kürşad Turgay, E-mail: turgay@mpusp.mpg.de

Abstract

Initiation of bacterial DNA replication takes place at the origin of replication, a region characterized by the presence of multiple DnaA boxes that serve as the binding sites for the master initiator protein DnaA. The absence or failure of DNA replication can result in bacterial cell growth arrest or death. Here, we aimed to uncover the physiological and molecular consequences of stopping replication in the model bacterium *Bacillus subtilis*. For this purpose, DNA replication was blocked using a CRISPRi approach specifically targeting DnaA boxes 6 and 7, which are essential for replication initiation. We characterized the phenotype of these cells and analyzed the overall changes in the proteome using quantitative mass spectrometry. Cells with arrested replication were elongating and not dividing but showed no evidence of DNA damage response. Moreover, these cells did not cease translation over time. This study sets the ground for future research on non-replicating but translationally active *B. subtilis*, which might be a valuable tool for biotechnological applications.

Importance

Even though bacteria are constantly replicating under laboratory conditions, natural environments expose them to various stresses like lack of nutrients, high salinity, and pH changes, which can keep them in non-replicating states. Non-replicating states can allow bacteria to become less sensitive or tolerant to antibiotics (persisters), remain inactive in specific niches for an extended period (dormancy), and adapt to some hostile ecosystems. Non-replicating states have been studied due to the possibility of repurposing energy to produce additional metabolites or proteins. Using CRISPRi targeting bacterial replication initiation sequences, we successfully arrested the

replication of *B. subtilis*. We observed that non-replicating cells continued growing but not dividing, and the initial arrest did not induce global stress conditions such as SOS or stringent response. Notably, these cells continued their metabolic activity and translation. This study provides comprehensive insights into the physiological response of replication initiation blockage in *B. subtilis*.

Introduction

DNA replication aims to duplicate the genomes of dividing cells to contribute a new identical DNA copy to each daughter cell. Replication is therefore connected to cell growth, chromosome segregation, and cell division. In bacteria, replication initiates at a specific part of the chromosome, the origin of replication (*oriC*). This region contains several DNA sequences called DnaA boxes that serve as binding sites for the master initiator protein DnaA. DnaA binds to several boxes at the *oriC*, causing the unwinding of an AT-rich region within the *oriC* and facilitating the recruitment of the replication machinery at both strands (1–4). The absence or failure of DNA replication can lead to bacterial growth arrest or cell death. Although bacteria can rapidly divide and replicate under laboratory conditions, most bacteria in their natural habitat encounter multiple stresses, such as nutrient scarcity, that hinder the capacity to duplicate. One example of the non-replicative states in bacteria is persister cells, which constitute a small percentage of the bacterial population that stops growing and is, therefore, less sensitive to antibiotics (5). Another example is the "oligotrophic growth state", in which bacteria can survive for multiple days in pure water while maintaining basic metabolic activities (6).

70 The physiology of non-growing bacteria has been studied due to its relevance in
71 industrial and clinical contexts (7). The main advantage of using these cells in industry
72 biotechnology is that the carbon and energy spent for biomass formation can be
73 redirected to produce compounds of interest (8, 9). Notably, metabolically active states
74 in non-growing bacteria have previously been reported, with some displaying
75 enhanced protein production (10–13). The methods to induce these non-replicating
76 states include, for example: **i)** the use of toxins from toxin-antitoxin systems to induce
77 a persister-like phenotype (14, 15), **ii)** exploiting repressible promoters to
78 downregulate the RNA polymerase (10), **iii)** the elimination of chromosomal content
79 with endonucleases such as I-CeuI (11), **iv)** the removal of the *oriC* with serine
80 integrases (16), **v)** mimicking nutrient depletion, the addition of growth inhibitors, and
81 the use of CRISPRi to knockdown genes related to growth or replication (8, 9, 17, 18).
82 In this study, we constructed a strain with a chromosomally integrated CRISPRi
83 system specifically targeting DnaA boxes 6 and 7, which have been previously
84 reported to be the most important to promote DNA unwinding during replication
85 initiation in *B. subtilis* (19). We characterized the phenotype upon CRISPRi induction
86 by evaluating cell morphology, membrane integrity, replication status, and SOS
87 response. The time-resolved quantitative proteome profile of this strain reveals a
88 significant change in the abundance of ribosomal proteins; however, SOS response
89 proteins are not significantly elevated. This indicates that these cells stop replicating
90 but continue growing and translating. Overall, our results shed light on the fundamental
91 role of replication initiation in *B. subtilis* and provide a foundation for subsequent
92 biotechnological studies of this bacterium as a producer strain.
93
94

95 **Results**

96 **An inducible CRISPRi system to block replication initiation**

97 A recent study showed that the DnaA boxes 6 and 7 on the *oriC* of *B. subtilis* are
98 crucial for DNA unwinding and replication initiation (19). Thus, we hypothesized that
99 initiation could be blocked by sterically hindering the binding of DnaA to these boxes
100 using a xylose-inducible dCas9 (18) (Fig. 1A). As a control, we also selected sgRNAs
101 targeting boxes 1 – 2 and 3 – 4 (sgRNA^{box1-2} and sgRNA^{box3-4}) (Fig. 1B). This system
102 allows the conditional expression of dCas9 when xylose is present in the medium but
103 also tight repression of it when glucose is present.

104 To assess the block of replication initiation, we evaluated the growth of cells in the
105 early logarithmic phase under induction or repression of dCas9. Cells carrying only the
106 dCas9 integration grew similarly in inducing and repressing conditions, meaning that
107 dCas9 expression alone does not alter the capacity of bacteria to proliferate (Fig. 1C).
108 Repressed cultures of the sgRNA^{box1-2} and sgRNA^{box3-4} had slight growth differences
109 compared to the control (Fig. 1C). Inducing dCas9 in the strain containing the
110 sgRNA^{box6-7} leads to a significant decrease in CFU/ml after 3 h. On the contrary, we
111 did not observe growth inhibition when the CRISPRi system targeted the other
112 adjacent boxes (Fig. 1C). This indicates that the observed effect results from a
113 competition between DnaA and dCas9 for binding to the DnaA boxes 6 and 7. This
114 specific block by the dCas9-sgRNA^{box6-7} complex could prevent DnaA-filament
115 formation and the subsequent associated replication-bubble opening that starts
116 replication. These observations also confirm the high specificity of DnaA binding to
117 certain boxes, specifically DnaA boxes 6 and 7, as an initial start of replication
118 initiation, as previously reported (19).

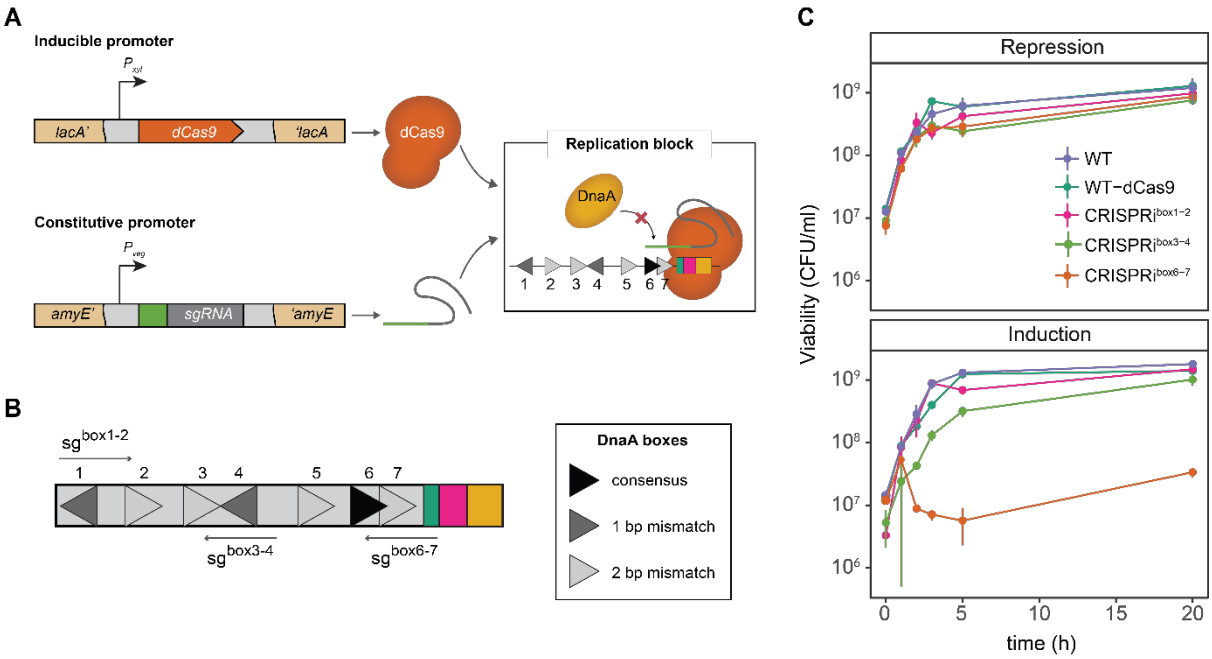

Figure 1: CRISPRi targeting the DnaA boxes 6-7 inhibit cell proliferation

(A) *B. subtilis* carrying a xylose-inducible dCas9 (orange) is directed to specific DNA targets by constitutively expressed sgRNAs (green) under the P_{veg} promoter control. The dCas9-sgRNA complex blocks the binding of DnaA (yellow) to the DnaA boxes (triangles). *dcas9* was stably integrated into the *lacA* locus, and the sgRNAs were integrated into the *amyE* locus. (B) DnaA boxes from *B. subtilis* and the selected sgRNA targets (left side). Other elements of the *oriC* are represented: DnaA trios (green), DnaD binding sites (fucsia) and the AT-rich region (yellow). (C) $CRISPRi^{box6-7}$ does not resume growth when induced at the early exponential growth phase. Cell counts of cells under repression (glucose) or induction (xylose) conditions. Data shown is the mean of 3 experiments and the error bars represent the SD.

CRISPRi system inhibits the initiation of replication, leading to replisome disassembly

To verify the effect of CRISPRi blocking replication initiation at single cell level, we followed the replisome localization by generating a translational fluorescent reporter gene fusion to the gene encoding the beta clamp of the polymerase protein, DnaN, at its endogenous genomic locus. DnaN colocalizes with the replisome making it an

137 excellent reporter to evaluate the progression of DNA replication in the cell (20). The
138 GFP-DnaN fusion protein forms bright foci that assemble and disassemble inside the
139 cells, signaling the start and completion of DNA replication, respectively. Previous
140 studies have shown that no DnaN foci form in the absence of replication, while actively
141 replicating cells contain between zero to four DnaN foci (20, 21).

142 Dynamic localization of GFP-DnaN was evaluated under xylose conditions (Fig. 2A).
143 The wild-type (WT) strain displayed bright foci, indicating that the replication forks are
144 assembled, and the cells are actively replicating. Remarkably, in strain CRISPRi^{box6-7},
145 foci diffusion is already observed after 2 hours of xylose induction, suggesting that
146 replication is no longer initiated in these cells.

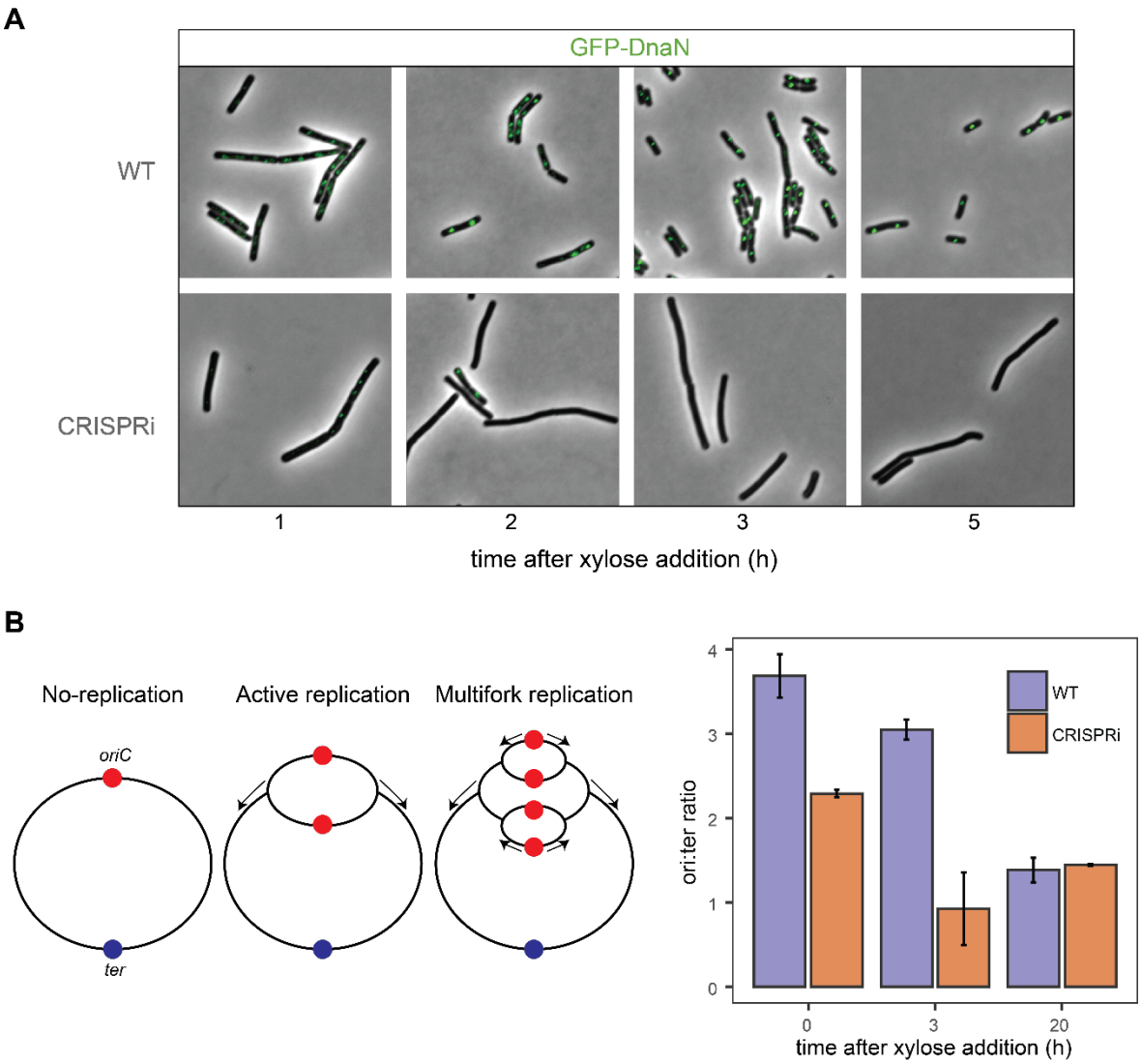

147

148 **Figure 2 Replication is inhibited in the CRISPRi strain.**

149 (A) Epifluorescence microscopy of *B. subtilis* cells expressing GFP-DnaN undergoing CRISPRi
150 replication arrest. Strains were grown in LB + 1% glucose until OD600nm 0.1, washed and resuspended
151 in LB + xylose 1%. Cells were immediately subjected to microscopic analysis at 1, 2 , 3 and 5 h after
152 xylose addition. (B) Left panel: Explanation of replication states in bacteria. In nutrient-rich conditions,
153 chromosomes undergo multifork replication and have more than one *oriC* (red) per cell; therefore, their
154 *ori* to *ter* (blue) ratio is higher than in non-replicating conditions. Right panel: ori:ter ratios as determined
155 by RT-qPCR for WT and CRISPRi cells. Data points in (B) represent the means of three independent
156 replicates; error bars indicate standard deviations of the mean.

157

158 Another method to demonstrate that replication initiation has stopped is analyzing the
159 frequency of the origin and terminus region (ori-ter ratio). Cells that are actively

160 replicating have a ratio above 1, while cells containing only one copy of the
161 chromosome, like stationary phase cells or in a non-replicating state, are expected to
162 have a ratio closer to 1 (Fig. 2B). We determined the ori-ter ratios using qPCR (Fig.
163 2B). We observed that blocking the DnaA boxes 6 and 7 resulted in a decreased DNA
164 replication initiation rate after 3 hours of induction with an ori:ter ratio of 0.88 vs 2.89
165 for WT cells. This demonstrates that replication is blocked by the designed system.
166 These observations are consistent with the inhibition of DNA replication initiation and
167 were confirmed by the observed replisome disassembly with the GFP-DnaN reporter.

168

169 **No evidence of DNA damage response under CRISPRi-mediated replication**
170 **arrest**

171 Bacteria can sense and respond to DNA stress through the widely conserved SOS
172 response (reviewed in (22, 23)). The SOS response initiates when single-stranded
173 DNA accumulates following DNA damage or replication blocks. One of the possible
174 consequences of inducing replication arrest in a rich medium is the occurrence of
175 replication-transcription conflicts at stalled replication forks resulting in DNA damage
176 (24). In *B. subtilis*, the protein involved in inhibiting cell division during the SOS
177 response is YneA (25), whose expression is repressed by LexA, the transcriptional
178 repressor of the SOS regulon (26).

179 To test whether the replication-arrested cells were undergoing DNA damage response
180 (DDR), we added an ectopic integration of *gfp* under the control of the *yneA* promoter
181 in the CRISPRi and WT background strains. Since DNA damage leads to de-
182 repression of genes controlled by LexA such as *yneA* (27), we used GFP expression
183 as an indicator of SOS response. For this, the GFP fluorescence of the cells was
184 observed at various timepoints after xylose addition. As a positive control, we

185 performed the same experiment but exposed the cells to mitomycin C, a DNA-
186 damaging agent which creates interstrand cross-links, induces the SOS response and
187 results in cell elongation (25).
188 Both WT and CRISPRi strains showed no signs of DDR using the P_{yneA}-GFP reporter
189 compared to the mitomycin DDR response in WT cells (Fig. 3A). This observation
190 indicates that the SOS response was not induced during CRISPRi-mediated
191 replication arrest.
192

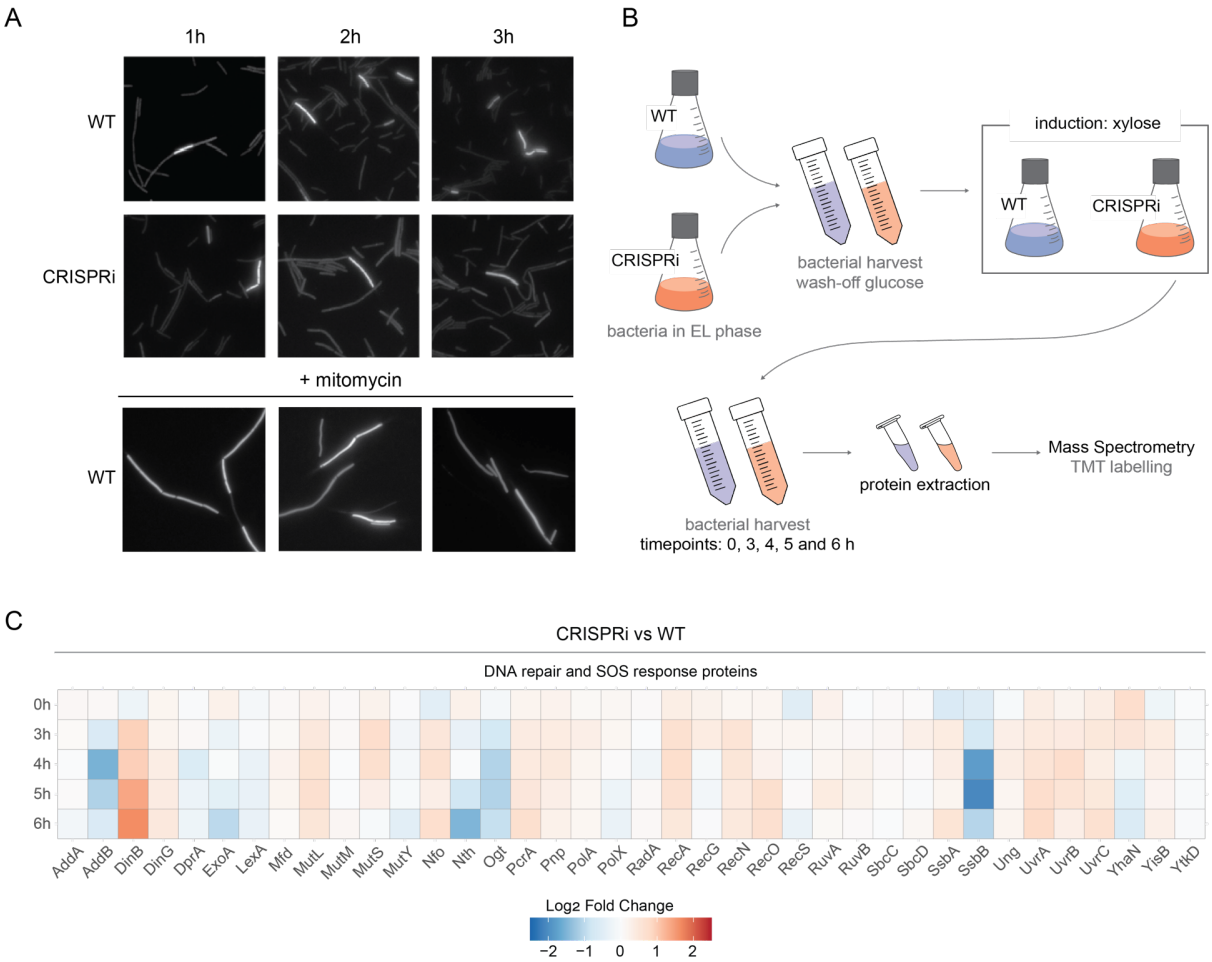

193
194 **Figure 3. No evidence of DNA damage under replication arrest**
195 (A) WT and CRISPRi strains containing the P_{yneA}-*gfp* ectopic integrations and grown LB with 1% xylose.
196 Images are from aliquots taken from cultures constantly growing at 37°C. Cells were subjected to
197 microscopic analysis at 1, 2 and 3 h after xylose addition. (B) An overview of the experimental setup to
198 collect the samples for MS analysis. WT and CRISPRi cells were harvested at different timepoints after

199 xylose induction, and their proteins were extracted and quantified by Tandem Mass Tag (TMT) mass
200 spectrometry. EL: Early logarithmic phase. (C) Heatmap based on Fold Change values of selected
201 proteins. DNA repair and SOS response-associated proteins are retrieved from SubtiWiki. Data
202 selected presents mean of 3 biological replicates.
203
204 To explore the response of *B. subtilis* to CRISPRi-mediated replication arrest over
205 time, we analyzed the overall proteome for differences between CRISPRi and WT
206 samples using quantitative mass spectrometry (Fig. 2B).
207 We observed almost no difference in the protein abundance profiles between
208 replicating cells (WT) and non-replicating cells (CRISPRi) at timepoint 0 h and clear
209 changes in differentially expressed proteins over the course of the experiments (Fig.
210 S1). Additionally, we observed that the DNA repair and SOS response proteins of
211 CRISPRi vs. WT did not show clear differences except for the nuclease inhibitor DinB,
212 which is differentially more abundant under replication arrest (Fig. 3C). These two
213 observations add further evidence that there is no significant DNA damage response
214 in the replication-arrested cells.
215
216 **CRISPRi-mediated replication arrest enhances protein expression**
217 To obtain a global view of the change in cellular processes upon replication arrest, we
218 analyzed the enrichment of the Gene Ontology (GO) terms within these cells (Fig. 4A
219 and Fig. S2). Here, we observed that after 5 and 6 h of replication arrest, the ribosomal
220 proteins and other translation-related proteins were more abundant. Our analysis
221 indicated no enrichment of SigB-regulated general stress response proteins (Fig. S3).

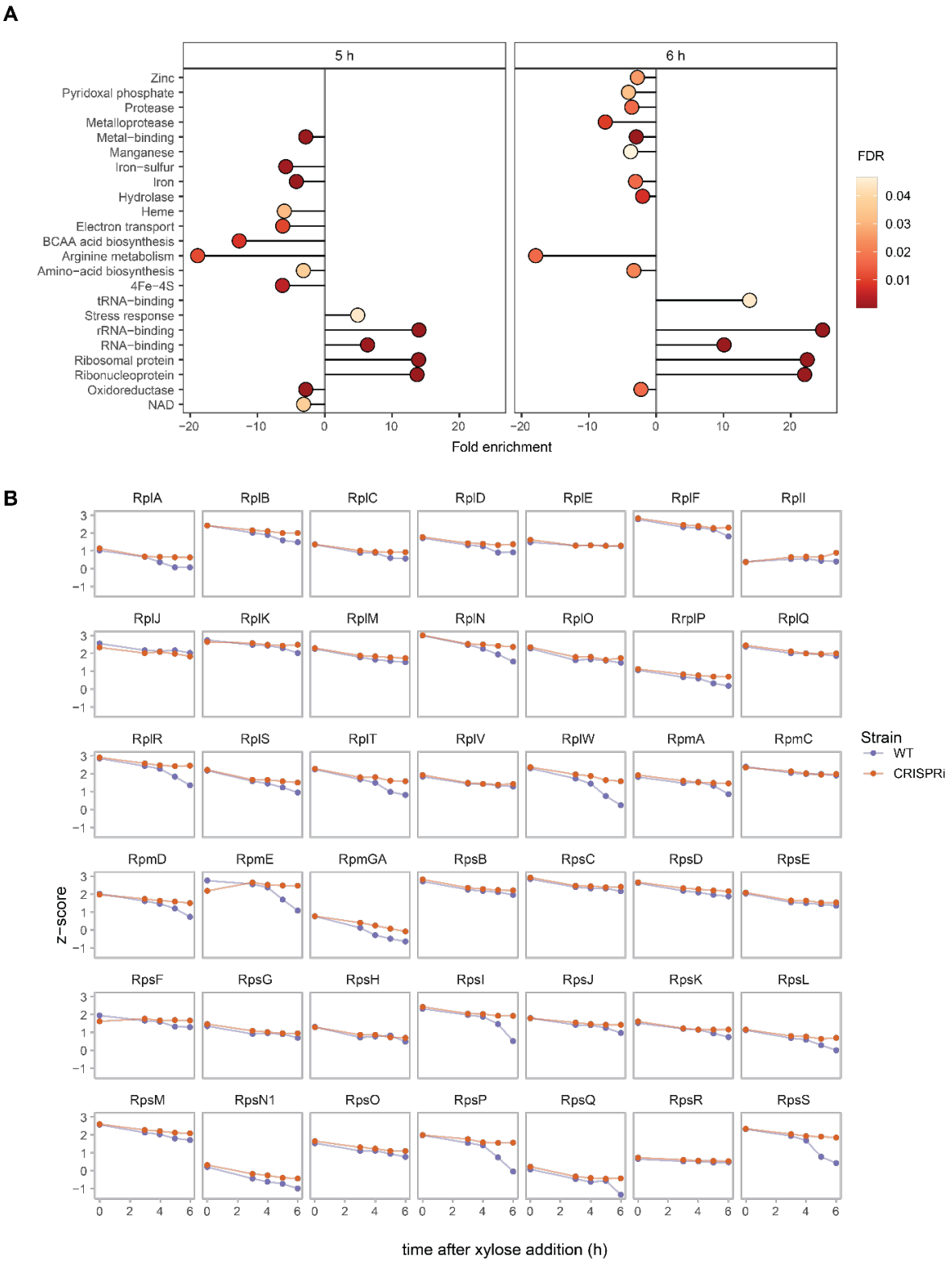

Figure 4. Proteomic characterization shows translation-related proteins are more abundant in replication-arrested cells after 5 and 6 h of xylose induction

(A) GO enrichment analysis of differentially expressed genes in CRISPRi and WT strains. Proteins whose abundance was significantly changed were analyzed. The enriched terms after 5 and 6 h of

227 xylose induction are shown. Dot color relates to False discovery rate (FDR) values for each process.
228 (B) Profile plots of z-score ribosomal proteins retrieved from Subtiwiki. Purple line indicates WT and
229 yellow CRISPRi strain.
230
231 Enhanced translation upon replication arrest is a possible mechanism to
232 increase protein and metabolite production and has been studied in *E. coli* (8, 9, 28).
233 To observe whether the levels of translation-related proteins were increased upon
234 replication arrest in *B. subtilis*, we made individual profile plots of translation-related
235 proteins as a function of the z-score (Fig. 4B). We observed that the level of most
236 ribosomal proteins in the CRISPRi strain remains constant over time. In contrast,
237 protein levels in the WT cells decreased (Fig. 4B). Our interpretation of this result is
238 that as WT cells enter the stationary phase, CRISPRi cells appear to be in an extended
239 exponential phase from the moment the replication block with dCas9 happens.
240 Next, we wanted to assess if the ribosomal protein abundance was related to
241 an increased translation. Therefore, we generated an ectopic integration of *gfp* under
242 an IPTG inducible promoter ($P_{hyperspank}$) in the WT and CRISPRi background strains
243 as a reporter for protein translation. We then measured GFP fluorescence in a time-
244 lapse experiment after xylose and IPTG addition (Fig 5A). We note that the
245 cytoplasmic GFP signal allowed us as well to observe the general morphology of the
246 cells. WT cells showed clear cell division and septum formation. In contrast, CRISPRi
247 cells showed an elongated phenotype without an apparent septum (Fig. 5A). We next
248 quantified the fluorescence intensity of individual cells from the timelapse microscopy
249 experiment. We found that after 3 hours of xylose addition, CRISPRi cells displayed a
250 significantly enhanced GFP intensity per cell compared to the WT. These results at
251 the proteomic and single-cell levels indicate that replication arrest affects the overall

252 translation process. However, the observed increase in GFP expression might also be

253 caused by its stabilization.

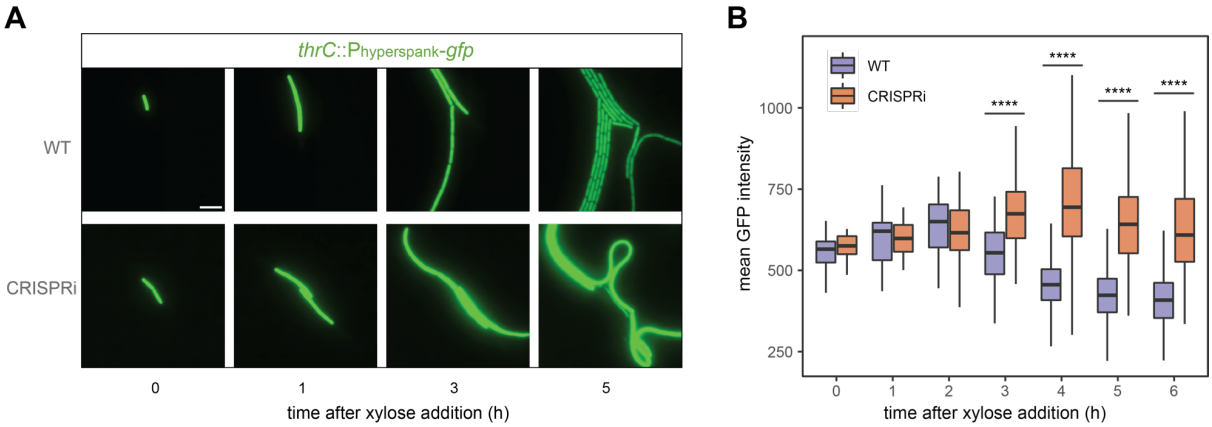

254

255 **Figure 5. Chromosomal GFP expression is higher after replication arrest.**

256 (A) Snapshots taken from a time-lapse microscopy experiment. An ectopic integration of *gfp* under an

257 IPTG inducible promoter was analyzed in the WT and CRISPRi background strains. Strains were grown

258 in the presence of both xylose and IPTG. CRISPRi cells showed an increase in fluorescence.

259 Representative pictures are shown. (B) Mean GFP intensity per cell upon xylose induction in WT and

260 CRISPRi cells. Two-tailed Welch tests were performed for CRISPRi against WT as a control group and

261 asterisk represent p-values. *: P ≤ 0.05, **: P ≤ 0.01, ***: P ≤ 0.001, ****:

262

263

264 **CRISPRi-mediated replication arrest causes cell elongation**

265 From the time-lapse experiment, we next quantified the cellular morphology after

266 inducing replication arrest. Overall, cells are larger during replication arrest in the

267 CRISPRi cells. These differences became significant already after 1 hour of xylose

268 induction and became even more significant after 2 hours of induction and throughout

269 the whole experiment (Fig. 6A).

270 To pinpoint specific proteins that can be enriched in the CRISPRi cells and explain the

271 elongated phenotype, we analyzed the protein abundance in our proteomic

272 experiment for other related processes like cell division, cell shape, and DNA

273 segregation (Fig. 6B). We observed that most proteins have similar cellular levels

274 compared to the WT. However, we found three related proteins: LytE, MreB, and
275 MreBH, to be differentially more abundant in CRISPRi (Fig. 6B). LytE is a cell wall
276 hydrolase involved in cell elongation and separation (29), whose activity requires
277 functional MreB and MreBH (30, 31). This observation suggested that uncontrolled
278 cell elongation might lead to cell lysis, which we observed after 7 hours of xylose
279 induction (Video S4).

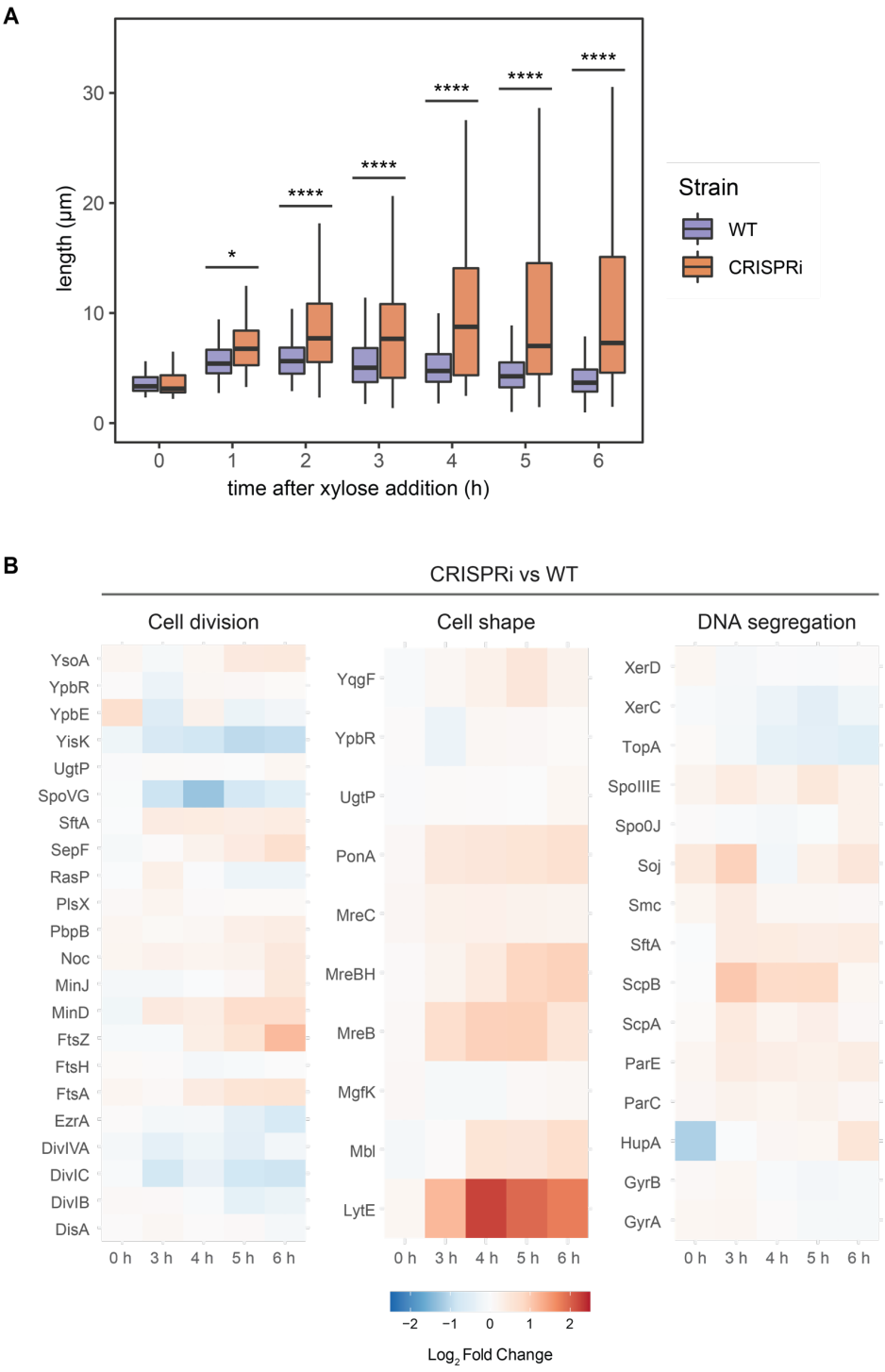

Figure 6. Uncontrolled cell elongation under replication arrest.

(A) Quantitative analysis of cell length on time-lapse data (Fig. 5). Cell length increases upon addition of xylose in CRISPRi cells. Data are represented as box plots with the mean cell length of all biological repeats. n =3. Two-tailed Welch tests were performed for CRISPRi against WT as a control group and asterisk represent p-values. *: P ≤ 0.05, **: P ≤ 0.01, ***: P ≤ 0.001, ****: P ≤ 0.0001. (B) Heatmap

286 based on Fold Change values of proteins related to cell division, cell shape and DNA segregation. All
287 proteins annotations are retrieved from SubtiWiki.
288
289 Taken together, these results show that CRISPRi mediated replication initiation arrest
290 is specific for the DnaA boxes 6 and 7. Moreover, this system stop the process of cell
291 division, while continuing the processes of cell translation and elongation. Additionally,
292 replication arrested cells do not undergo global stress response regulation.
293
294
295 **Discussion**

296 In this work, we employed a rational design using CRISPRi to block replication
297 initiation in *B. subtilis*. This block hinders the capacity of DnaA to bind specific DnaA
298 boxes, thereby impeding replication initiation but not interfering with DnaA expression
299 and its function as a transcriptional regulator (32). We found that targeting DnaA boxes
300 6 and 7 was more efficient than targeting other DnaA boxes within the *oriC* (Fig. 1C).
301 This finding aligns with previous reports targeting DnaA boxes in *B. subtilis* (19). In
302 contrast, targeting any DnaA box within the *oriC* in *E. coli* produces a non-replicating
303 phenotype (17). Based on these observations, we confirm that specific DnaA boxes
304 within the *oriC* in *B. subtilis* have a specialized function to trigger replication initiation.
305 However, it remains elusive whether such functional hierarchy in the DnaA boxes in
306 *B. subtilis* is observed in other bacteria. We expect this to be the case given the
307 conserved *oriC* architecture in *B. subtilis* and its similarities with other bacteria (33). It
308 is also interesting to know to what extent the location of *oriC* in *E. coli*, which is 40 kb
309 away from the DnaA and DnaN genes, might affect the functional hierarchy of the
310 DnaA boxes (33).

311 CRISPRi-mediated replication arrested cells were characterized by employing
312 cell biological assays in combination with proteomics approaches. We found that
313 CRISPRi-mediated block at the DnaA boxes 6 and 7 leads to a shutdown of the critical
314 cell cycle processes of DNA replication (Fig. 2) and cell division (Fig. 5A) while growth
315 (Fig. 5A and Fig. 6A) and translation continue (Fig. 4A and Fig. 5B). The phenotype
316 observed under replication arrest, where cells stop dividing and form filaments is
317 characteristic of cells under the SOS response and is mediated by YneA (26).
318 However, profile plots of SOS-response-associated proteins indicate that this stress
319 response is not active (Fig. 3C). Moreover, the translational fusion of the *yneA*
320 promoter to GFP to detect the cellular SOS response did not show activity (Fig. 3A
321 and Fig. 3C).

322 Since the observed phenotype was not caused by the SOS-response, we think
323 this could indicate that the stop in cell division is SOS response independent. SOS-
324 independent inhibition of cell division has been reported in several microorganisms
325 (34–36). Likewise, DnaA binds specifically to the promoter regions of several genes,
326 including *ftsL* (32). FtsL is an unstable protein and is essential for cell division (34). A
327 decrease in *ftsL* mRNA levels quickly causes a decrease in FtsL protein and inhibits
328 cell division (25, 37). Future work can pinpoint at the specific response that halts
329 division by following the promoter activity or the expression of those genes in non-
330 replicating cells.

331 Proteomic analysis of the non-replicating cells revealed that proteins involved
332 in translation (rRNA-binding, ribosomal proteins, tRNA-binding and nucleoproteins)
333 are more abundant after 5 and 6 hour of xylose addition compared to WT (Fig. 4A).
334 Studies in several bacteria have suggested that protein synthesis continues during
335 growth arrest and that maintaining functional translation machinery may be required

336 for their viability (10–12, 38). Additionally, several studies in *E. coli* demonstrated
337 enhanced protein and biochemical production of proteins and metabolites during
338 replication arrest (8, 9, 28). We further confirmed that non-replicating cells maintained
339 a higher rate of protein expression than WT cells (Fig. 5).

340 While the effect of protein expression is enhanced as described in other
341 organisms, replication arrested *B. subtilis* cells started to lyse after 7 hours of induction
342 (Video S1) probably because of the uncontrolled elongation of the cells. Cell
343 elongation has been previously reported in some temperature-sensitive mutants for
344 replications initiation in *B. subtilis* (39–41) and CRISPRi-mediated replication arrest in
345 *E. coli* (17). However, these studies did not address if the uncontrolled elongation
346 results in cell lysis. These elongation effects may be bypassed by making the process
347 reversible before cell lysis (on/off switch of replication arrest) using temperature
348 switches (42), degradation tags (17), light-activated and sensitive variants (42–44), or
349 split variants (45).

350 For future biotech applications of these replication inhibiting CRISPRi cells as
351 a microbial cell factory, it is important to effectively remove the need to add xylose in
352 the media to induce dCas9 and eliminate the cell elongation constraints. To address
353 the first, the expression of dCas9 can be driven by self-inducing promoters (46–48)
354 that remove the dependence on chemical inducers, which are not economical at
355 industrial scales. For the second, keeping control of the cell shape and membrane
356 homeostasis may extend the lifespan of the bacteria and avoid anticipated cell lysis
357 for industrial applications (24). One way to address this issue is to knockout elongation
358 proteins that are being overexpressed such as LytE (Fig. 6B). However, deletion of
359 cell wall hydrolases like LytE might not have an effect due to their redundancy, as
360 single knockouts present no phenotype. In a multiple knockout approach of *B. subtilis*

361 cell wall hydrolases (42 in total), researchers were able to remove all but two of these
362 genes in a single strain, *lytE* and *cwlO,* which were shown to be synthetically lethal
363 (49). Their results indicate that the only essential function of cell wall hydrolases in *B.*
364 *subtilis* is to enable cell growth by expanding the wall and that LytE or CwlO alone is
365 sufficient for this function. Therefore, we suggest building a library to screen for targets
366 that inhibit cell replication and growth while allowing for continued protein production.
367 Similar approaches have been performed in *E. coli* (9).

368 The current system also has some limitations. For instance, comparing the non-
369 replicating CRISPRi with the replicating WT cells is challenging. Over time, replicating
370 cells increase cell density, so their nutrient availability is exhausted faster than non-
371 replicating cells. Hence, up- or downregulation of specific metabolic pathways in
372 replicating cells could also be caused by nutrient limitation and the entry into stationary
373 phase. These concerns about a better-suited comparison of the two different cellular
374 states can be addressed in future work by using either a chemostat or microfluidic
375 approaches that can maintain the cells in similar growth states.

376 Finally, this system could become a source for producing many toxins and
377 antibiotics that target the DNA replication machinery. In conclusion, our results show
378 a phenotypic and proteomic characterization of an unusual cellular state of a
379 replication-arrested strain generated by specifically targeting DnaA boxes 6 and 7 with
380 CRISPRi, which disintegrates the replisome and in the inhibition of critical cell cycle
381 processes like DNA replication and cell division, while protein translation and cell
382 elongation persists.

383

384 **Materials and Methods**

385 **Strains and culture conditions**

386 Bacterial strains and vectors used in this study are listed in **Tables S1 and S2**.
387 *B. subtilis* and its derivative strains were routinely cultured in Luria-Bertani (LB Broth
388 Miller, Becton Dickinson) medium containing: 10 g/L tryptone, 5 g/L yeast extract, 10
389 g/L NaCl (and 15 g/L agar for solid medium) with constant shaking of 180-200 rpm at
390 37°C. In addition, LB was supplemented with glucose (1%) or xylose (1%) when
391 indicated. *E. coli* strains were grown at 37°C with constant shaking at 180 rpm in LB
392 or LB agar supplemented with the appropriate antibiotics for selection on plates.

393 *B. subtilis* was grown at 37°C on a LB agar plate streaked from bacteria glycerol
394 stocks stored at -80°C. Subsequently, cultures were grown from single colonies. When
395 needed, antibiotics were added to the media at the following final concentrations: 10
396 µg/ml kanamycin (CorningTM) and 1 µg/ml erythromycin (Sigma-Aldrich); 15 µg/ml
397 lyncomycin (CorningTM) and 150 µg/ml spectinomycin (Sigma-Aldrich) for *E. coli*.
398 Xylose was added to a final concentration of 1% (w/w) to induce the conditional
399 promoter (P_{xylA}). Glucose was used at a final concentration of 1% (w/v) and was used
400 to repress the conditional inducible xylose inducible promoter (P_{xylA}).

401

402 **Serial dilution plating viability assay**

403 Overnight cultures were diluted to $OD_{600\ nm}$ 0.01 in 20 ml LB with 1% glucose in
404 100 ml flasks and further incubated at 37°C, 180 rpm until $OD_{600\ nm}$ 0.25 (+/- 0.025).
405 To ensure cells are in early exponential phase, cultures were then back-diluted 1:10
406 in a total volume of 120 ml LB and 1% glucose in 1 L flasks, incubated at 37°C, 180
407 rpm until $OD_{600\ nm}$ 0.1 (+/- 0.025). Cells were pelleted at 4000g, at room temperature

408 for 5 min and resuspended in LB supplemented with either 1% glucose or 1% xylose.
409 Cells were incubated at 37°C, 180 rpm and 100 µl samples were taken at 0, 1, 3 and
410 20 h and then 10-fold serially diluted in LB. 5 µl of each dilution was spotted onto LB
411 agar plates containing 1% (w/v) glucose to inhibit additional expression of dCas9 and
412 incubated overnight at 37°C. The number of CFU/ml was monitored.

413

414 **Determination of origin-to-terminus ratio by qPCR**

415 Cells in early logarithmic phase ($OD_{600\ nm}$ 0.1 ± 0.025) were pelleted at 4000 *g*,
416 at room temperature for 5 min, split in two and resuspended either in LB supplemented
417 with 1% glucose or 1% xylose and incubated at 37°C, 180 rpm. 15 ml samples were
418 taken at different time points (0, 3 and 20 hours), spun down at 11000 *g*, 4°C for 5 min
419 followed by a genomic DNA extraction with the Nucleospin DNA extraction Kit
420 (macherey-nagel) according to the manufacturer's instructions.

421 The primer pair targeting the origin region was OLEC11491 and OLEC11492,
422 and for the terminus was OLEC11493 and OLEC11494. qPCR reactions of 20 µl
423 contained 2.5 ng of DNA, 200 nM of each primer and 10 µl of 2X Power SYBR™ Green
424 PCR-Master-Mix (Applied Biosciences™), and amplifications were performed on a
425 QuantStudio™ 5 Real-Time PCR system (Applied Biosciences) according to the
426 following protocol: 95°C for 3 min, followed by 40 cycles of 95°C for 30 s, 60°C for 30
427 s and 72°C for 30 s. ori-ter ratios were analyzed using the 2ΔΔCt method(50). A fixed
428 sample of the WT strain grown into late stationary phase, where the population would
429 be expected to have an ori-ter ratio corresponding to 1, was used for normalization in
430 every cycling run.

431

432 **Replisome localization by GFP-DnaN**

433 Cell in early logarithmic phase were pelleted at 4000 g, at room temperature for
434 5 min and resuspended in LB supplemented with either 1% glucose or 1% xylose.
435 Afterwards, they were incubated at 37°C, 180 rpm and 200 µl samples from timepoint
436 1, 2, 3 and 5 h were spun down at RT, 4000 g for 5 min. Cell pellets were washed
437 twice with 1X PBS and resuspended in a final volume of 500 µl 1X PBS from which
438 1.5 µl were spotted onto 1.5% agarose pads and observed under the microscope using
439 the GFP channel.

440

441 **DNA damage response assay**

442 The promoter of *yneA* was fused to *gfp* gene and integrated into the ectopic
443 *amyE* locus (27). Strains in early logarithmic growth phase ($OD_{600\ nm}$ 0.1) were treated
444 with 1% glucose to repress or 1% xylose to induce expression of dCas9 for 3 hours.
445 Cells treated with 3 µg/ml mitomycin for 3 hours were used as positive controls. 1 ml
446 of each culture was washed twice (4000 *g*, room temperature for 5 min) and
447 suspended in 1X PBS (phosphate-buffered saline, NaCl 137 mM, KCl 27 mM,
448 Na_2HPO4 10 mM, KH_2PO_4 1.8 mM, pH 7.4); 2 µl were placed on 1.5% agarose in TAE
449 pads.

450

451 **Fluorescence microscopy**

452 Cell were grown to an $OD_{600\ nm}$ of ~0.4. One microliter of cells was spotted onto
453 1.5% agarose pads and imaged. Images were acquired with an Inverted Microscope
454 (Leica DMi8, DFC9000 GT VSC-D6212 camera), and a 100× phase contrast objective
455 (HC LP APO 100X/1.40 oil). Filter sets for GFP channel were used when indicated.

456

457 **Time-lapse microscopy**

458 After preparation of the culture, bacterial samples were added to an 1%
459 agarose pad in $S_{7\ 50}$ media (51) supplemented with IPTG (1mM) and 1% xylose.
460 Fluorescence time-lapse microscopy was carried out using a Ti-2 Nikon inverted
461 microscope equipped with a CFI Plan Apochromat DM 60× Lambda oil Ph3/1.40
462 objective (Nikon) and camera Fusion FT (12bit sensitive scan mode standard,
463 Hamamatsu) in the absence of binning. A denoise module (Nikon) was used during
464 the acquisition of the images. Microscope settings were set to the following: GFP 488
465 nm 50ms 5%, Phase Contrast: 150ms DIA 12bit sensitive single plane, using a LED
466 Lamp Lumencor Spectra III light engine (Lumencor) and filter cube MXR00256 - LED-
467 DA/FI/TR/Cy5/Cy7-A (DAPI / FITC / TRITC / Cy5 / Cy7 - Full Multiband Penta)
468 (Semrock). Images were taken every 10 minutes in a pre-warmed chamber at 37°C
469 with Nikon Perfect Focus Systems (PFS4).

470 Image analysis was performed using Fiji (52) and ilastik (53) to segment the
471 cells, and MicrobeJ (54) to subsequently detect the cells and analyse the mean GFP
472 fluorescence intensities and cell length. For each strain, three positions on the agarose
473 pad were imaged and analysed.

474

475 **Identification and quantification of proteins by mass spectrometry**

476 *Sample collection*

477 Strains were grown in LB and 1% glucose. Once they reach early logarithmic
478 phase cells pelleted at 4000 *g*, at room temperature for 5 min and resuspended in LB
479 supplemented with 1% xylose. Cells were incubated at 37°C, 180 rpm and 20 ml
480 samples were taken at different timepoints per treatment (0, 3, 4, 5 and 6 hours)
481 followed by centrifugation at 11,000 *g*, 4°C for 5 min. Pellets were resuspended in 20
482 ml of ice-cold 1X PBS.

483 Cells were lysed with 500 µl 2x lysis buffer (final concentration: 2% SDS, 20
484 mM TCEP, 80 mM CAA (Chloroacetamide, Sigma-Aldrich), 100 mM HEPES pH 8
485 (VWR), 0.5x protease inhibitors (Roche) in tubes containing 25 mg 0.1mm silica beads
486 (BeadBeater® Glass beads, 0.1 mm (Roth) and were disrupted using a FastPrep-
487 24TM 5G Homogenizer (MP Biomedicals). Samples were spun down at 11000 g, 10
488 min to separate the soluble from the insoluble fraction. The supernatant was heated
489 at 95°C for 5 min and then cooled down to room temperature. The protein
490 concentration was determined using Pierce™ BCA Protein Assay Kit (ThermoFisher
491 Scientific), followed by nucleic acid digestion with 0.5 Units of Benzonase per 1 µg of
492 protein (Sigma-Aldrich) for 30 min at 37°C. Samples were kept at -20°C for further
493 analyses.

494

495 *Sample preparation*

496 All samples were subjected to SP3 sample preparation(55) on an Agilent
497 BRAVO liquid handling robot. Ten µg of a 1:1 mixture of hydrophilic and hydrophobic

498 carboxyl-coated paramagnetic beads (SeraMag, #24152105050250 and
499 #44152105050250, GE Healthcare) were added for each µg of protein. Protein binding
500 was induced by addition of acetonitrile to a final concentration of 50% (v/v). Samples
501 were incubated for 10 min at room temperature. The tubes were placed on a magnetic
502 rack, and beads were allowed to settle for 3 min. The supernatant was discarded, and
503 beads were rinsed three times with 200 µL of 80% ethanol without removing the tubes
504 from the rack. Beads were resuspended in digestion buffer containing 50 mM
505 triethylammonium bicarbonate and both Trypsin (Serva) and Lys-C (Wako) in a 1:50
506 enzyme to protein ratio. Protein digestion was carried out for 14 hours at 37°C in a
507 PCR cycler. Afterwards the supernatant was recovered dried down in a vacuum
508 concentrator.

509

510 *Peptide labeling and fractionation*

511 TMT 11plex (Pierce, #A37725) was used for peptide multiplexing and
512 quantification. Briefly, equal amounts of peptides were resuspended in 50 mM HEPES
513 pH 8.5. Additionally, 10% from each sample was pooled to create a common sample
514 as internal standard. TMT reagents were allowed to equilibrate to room temperature
515 for 30 minutes and were dissolved in anhydrous acetonitrile to a final concentration of
516 59 mM. To each sample TMT was added to a final concentration of 11.8 mM and tubes
517 were incubated at 25°C for 60 minutes with mixing at 500 rpm on a ThermoMixer.
518 Labeling was quenched by addition of hydroxylamine to a final concentration of 0.4%.
519 Samples were mixed, desalted using solid phase extraction (Seppak 1cc/50mg,
520 Waters), dried down in a vacuum concentrator and resuspended in 20 µL 2%
521 acetonitrile. Basic reversed phase fractionation was performed on a quaternary Agilent

522 1290 Infinity II UPLC system equipped with a Kinetex Evo-C18 column (150 x 2.1 mm,
523 2.6µm, 100 Å, Phenomenex) that was operated at 40°C. Solvent A consisted of HPLC
524 grade water, solvent B consisted of 100% acetonitrile, and solvent C consisted of 25
525 mM ammoniumbicarbonate in water. Fractionation was carried out at a constant flow
526 rate of 100 µl/min using a linear gradient from 2-25% acetonitrile within 50 minutes,
527 followed by column washing and equilibration. Over the whole gradient solvent C was
528 kept constant at 10%. In total 32 fractions were collected in conical 96well plates. The
529 organic solvent was removed in a vacuum concentrator for 30 minutes and fractions
530 were concatenated into 8 final samples. Peptides were acidified with formic acid,
531 desalted using OASIS HLB 96well cartridges (Waters, #186001828BA), dried down
532 and resuspended in 2% acetonitrile, 0.1% trifluoroacetic acid (TFA) prior MS analysis.

533

534 *Mass spectrometry*

535 All samples were analyzed on a Orbitrap Exploris (Thermo Scientific) that was
536 coupled to a 3000 RSLC nano UPLC (Thermo Scientific). Samples were loaded on a
537 pepmap trap cartridge (300 µm i.d. x 5 mm, C18, Thermo) with 2% acetonitrile, 0.1%
538 TFA at a flow rate of 20 µL/min. Peptides were separated over a 50 cm analytical
539 column (Picofrit, 360 µm O.D., 75 µm I.D., 10 µm tip opening, non-coated, New
540 Objective) that was packed in-house with Poroshell 120 EC-C18, 2.7 µm (Agilent).
541 Solvent A consists of 0.1% formic acid in water. Elution was carried out at a constant
542 flow rate of 250 nL/min using a 180 minute method: 8-33% solvent B (0.1% formic acid
543 in 80% acetonitrile) within 120 minutes, 33-48% solvent B within 25 minutes, 48-98%
544 buffer B within 1 minute, followed by column washing and equilibration. Data
545 acquisition on the Orbitrap Exploris was carried out using a data-dependent method

546 in positive ion mode. MS survey scans were acquired from 375-1500 m/z in profile
547 mode at a resolution of 120,000. AGC target was set to 100% at a maximum injection
548 time of 50 ms. The ten most abundant peptides were isolated within a 0.4 m/z window
549 and subjected to HCD fragmentation at a normalized collision energy of 36%. The
550 MS2 AGC target was set to 200%, allowing a maximum injection time of 54 ms.
551 Product ions were detected in the Orbitrap at a resolution of 30,000. TurboTMT
552 acquisition as enabled. Precursors were dynamically excluded for 45 s.

553

554 *Data analysis*

555 Data analysis performed as described in Schäfer and collaborators (56). A two-tailed
556 t-test and *p*-value correction were performed using Perseus to identify differentially
557 expressed proteins ($|\log_2$ fold change$| \geq 1$; *p*-value ≤ 0.05). Enriched pathways,
558 biological processes and Uniprot keywords were calculated using DAVID (57, 58).

559 Proteins forming part of the ribosome or involved in cell length, shape, or cell
560 division used for profile plots and heat maps were retrieved from SubtiWiki (59). The
561 log2 protein intensities were scaled to standard deviation units (*z*-scores) using R for
562 profile plots.

563 The mass spectrometry proteomics data have been deposited to the
564 ProteomeXchange Consortium via the PRIDE (60) partner repository.

565 **Acknowledgements**

566 We acknowledge Prof. Heath Murray from the Newcastle University for strains and
567 valuable discussions. We thank Tim Sullivan for support with sgRNA off-target scoring.
568 The authors are grateful to the members of the Charpentier group for constructive

discussions and critical reading of the paper. This work was supported by the Max Planck Society [to M.E. and E.C.], the Max Planck Foundation [E.C.], Deutsche Forschungsgemeinschaft (DFG) [Leibniz-Prize to E.C.] and the Volkswagen Stiftung [to A.K.W.E.].

Contributions

V.M.G, A.K.W.E., K.T., F.A.C., C.K.F. and E.C. designed the study; V.M., K.S., C.K.F and M.H. performed the experiments; F.A.C., M.H., C.K.F. and V.M.G performed the data analysis; V.M.G., F.A.C., M.H. and A.K.W.E. interpreted the data; A.K.W.E., K.T., M.E., and E.C. oversaw the project; V.M. wrote the paper. All the authors read, edited, and approved the paper.

References

1. Mott ML, Berger JM. 2007. DNA replication initiation: mechanisms and regulation in bacteria. Nat Rev Microbiol 5:343–354.

2. Katayama T, Ozaki S, Keyamura K, Fujimitsu K. 2010. Regulation of the replication cycle: conserved and diverse regulatory systems for DnaA and oriC. Nat Rev Microbiol 8:163–170.

3. Leonard AC, Grimwade JE. 2011. Regulation of DnaA assembly and activity: taking directions from the genome. Annu Rev Microbiol 65:19–35.

589 4. Richardson TT, Harran O, Murray H. 2016. The bacterial DnaA-trio replication
590 origin element specifies single-stranded DNA initiator binding. Nature 534:412–
591 416.

592 5. Balaban NQ, Helaine S, Lewis K, Ackermann M, Aldridge B, Andersson DI,
593 Brynildsen MP, Bumann D, Camilli A, Collins JJ, Dehio C, Fortune S, Ghigo J-M,
594 Hardt W-D, Harms A, Heinemann M, Hung DT, Jenal U, Levin BR, Michiels J,
595 Storz G, Tan M-W, Tenson T, Van Melderen L, Zinkernagel A. 2019. Definitions
596 and guidelines for research on antibiotic persistence. Nat Rev Microbiol 17:441–
597 448.

598 6. Gray DA, Dugar G, Gamba P, Strahl H, Jonker MJ, Hamoen LW. 2019. Extreme
599 slow growth as alternative strategy to survive deep starvation in bacteria. Nat
600 Commun 10:890.

601 7. Lempp M, Lubrano P, Bange G, Link H. 2020. Metabolism of non-growing
602 bacteria. Biol Chem 401:1479–1485.

603 8. Li S, Jendresen CB, Grünberger A, Ronda C, Jensen SI, Noack S, Nielsen AT.
604 2016. Enhanced protein and biochemical production using CRISPRi-based
605 growth switches. Metab Eng 38:274–284.

606 9. Li S, Jendresen CB, Landberg J, Pedersen LE, Sonnenschein N, Jensen SI,
607 Nielsen AT. 2020. Genome-Wide CRISPRi-Based Identification of Targets for
608 Decoupling Growth from Production. ACS Synth Biol 9:1030–1040.

609 10. Gefen O, Gabay C, Mumcuoglu M, Engel G, Balaban NQ. 2008. Single-cell
610 protein induction dynamics reveals a period of vulnerability to antibiotics in
611 persister bacteria. Proc Natl Acad Sci U S A 105:6145–6149.

612 11. Gefen O, Fridman O, Ronin I, Balaban NQ. 2014. Direct observation of single
613 stationary-phase bacteria reveals a surprisingly long period of constant protein
614 production activity. PNAS 111:556–561.

615 12. Manina G, Dhar N, McKinney JD. 2015. Stress and host immunity amplify
616 Mycobacterium tuberculosis phenotypic heterogeneity and induce nongrowing
617 metabolically active forms. Cell Host Microbe 17:32–46.

618 13. Yin L, Ma H, Nakayasu ES, Payne SH, Morris DR, Harwood CS. 2019. Bacterial
619 Longevity Requires Protein Synthesis and a Stringent Response. mBio 10.

620 14. Bokinsky G, Baidoo EEK, Akella S, Burd H, Weaver D, Alonso-Gutierrez J,
621 García-Martín H, Lee TS, Keasling JD. 2013. HipA-triggered growth arrest and β-
622 lactam tolerance in Escherichia coli are mediated by RelA-dependent ppGpp
623 synthesis. J Bacteriol 195:3173–3182.

624 15. Shomar H, Gontier S, van den Broek NJF, Tejeda Mora H, Noga MJ, Hagedoorn
625 P-L, Bokinsky G. 2018. Metabolic engineering of a carbapenem antibiotic
626 synthesis pathway in Escherichia coli. Nat Chem Biol 14:794–800.

627 16. Kasari M, Kasari V, Kärmas M, Jõers A. 2021. Decoupling growth and production
628 by removing the origin of replication from a bacterial chromosome. bioRxiv
629 2021.12.07.471534.

630 17. Wiktor J, Lesterlin C, Sherratt DJ, Dekker C. 2016. CRISPR-mediated control of
631 the bacterial initiation of replication. Nucleic Acids Res 44:3801–3810.

632 18. Peters JM, Colavin A, Shi H, Czarny TL, Larson MH, Wong S, Hawkins JS, Lu
633 CHS, Koo B-M, Marta E, Shiver AL, Whitehead EH, Weissman JS, Brown ED, Qi

634 LS, Huang KC, Gross CA. 2016. A Comprehensive, CRISPR-based Functional
635 Analysis of Essential Genes in Bacteria. Cell 165:1493–1506.

636 19. Richardson TT, Stevens D, Pelliciari S, Harran O, Sperlea T, Murray H. 2019.
637 Identification of a basal system for unwinding a bacterial chromosome origin.
638 EMBO J 38:e101649.

639 20. Goranov AI, Breier AM, Merrikh H, Grossman AD. 2009. YabA of Bacillus subtilis
640 controls DnaA-mediated replication initiation but not the transcriptional response
641 to replication stress. Mol Microbiol 74:454–466.

642 21. Soufo CD, Soufo HJD, Noirot-Gros M-F, Steindorf A, Noirot P, Graumann PL.
643 2008. Cell-cycle-dependent spatial sequestration of the DnaA replication initiator
644 protein in Bacillus subtilis. Dev Cell 15:935–941.

645 22. Friedberg EC. 2003. DNA damage and repair. Nature 421:436–440.

646 23. Janion C. 2008. Inducible SOS response system of DNA repair and mutagenesis
647 in Escherichia coli. Int J Biol Sci 4:338–344.

648 24. Merrikh H, Zhang Y, Grossman AD, Wang JD. 2012. Replication-transcription
649 conflicts in bacteria. Nat Rev Microbiol 10:449–458.

650 25. Kawai Y, Moriya S, Ogasawara N. 2003. Identification of a protein, YneA,
651 responsible for cell division suppression during the SOS response in Bacillus
652 subtilis. Mol Microbiol 47:1113–1122.

653 26. Au N, Kuester-Schoeck E, Mandava V, Bothwell LE, Canny SP, Chachu K,
654 Colavito SA, Fuller SN, Groban ES, Hensley LA, O'Brien TC, Shah A, Tierney JT,

655 Tomm LL, O'Gara TM, Goranov AI, Grossman AD, Lovett CM. 2005. Genetic
656 composition of the Bacillus subtilis SOS system. J Bacteriol 187:7655–7666.

657 27. Gozzi K, Ching C, Paruthiyil S, Zhao Y, Godoy-Carter V, Chai Y. 2017. Bacillus
658 subtilis utilizes the DNA damage response to manage multicellular development.
659 NPJ Biofilms Microbiomes 3:8.

660 28. Kasari M, Kasari V, Kärmas M, Jõers A. 2022. Decoupling Growth and Production
661 by Removing the Origin of Replication from a Bacterial Chromosome. ACS Synth
662 Biol https://doi.org/10.1021/acssynbio.1c00618.

663 29. Ishikawa S, Hara Y, Ohnishi R, Sekiguchi J. 1998. Regulation of a new cell wall
664 hydrolase gene, cwlF, which affects cell separation in Bacillus subtilis. J Bacteriol
665 180:2549–2555.

666 30. Domínguez-Cuevas P, Porcelli I, Daniel RA, Errington J. 2013. Differentiated
667 roles for MreB-actin isologues and autolytic enzymes in Bacillus subtilis
668 morphogenesis. Mol Microbiol 89:1084–1098.

669 31. Carballido-López R, Formstone A, Li Y, Ehrlich SD, Noirot P, Errington J. 2006.
670 Actin homolog MreBH governs cell morphogenesis by localization of the cell wall
671 hydrolase LytE. Dev Cell 11:399–409.

672 32. Washington TA, Smith JL, Grossman AD. 2017. Genetic networks controlled by
673 the bacterial replication initiator and transcription factor DnaA in Bacillus subtilis.
674 Mol Microbiol 106:109–128.

675 33. Briggs GS, Smits WK, Soultanas P. 2012. Chromosomal replication initiation
676 machinery of low-G+C-content Firmicutes. J Bacteriol 194:5162–5170.

677 34. Modell JW, Kambara TK, Perchuk BS, Laub MT. 2014. A DNA damage-induced,
678 SOS-independent checkpoint regulates cell division in Caulobacter crescentus.
679 PLoS Biol 12:e1001977.

680 35. Bojer MS, Frees D, Ingmer H. 2020. SosA in Staphylococci: an addition to the
681 paradigm of membrane-localized, SOS-induced cell division inhibition in bacteria.
682 Curr Genet 66:495–499.

683 36. Burby PE, Simmons LA. 2020. Regulation of Cell Division in Bacteria by
684 Monitoring Genome Integrity and DNA Replication Status. Journal of Bacteriology
685 202.

686 37. Goranov AI, Katz L, Breier AM, Burge CB, Grossman AD. 2005. A transcriptional
687 response to replication status mediated by the conserved bacterial replication
688 protein DnaA. Proc Natl Acad Sci U S A 102:12932–12937.

689 38. Stapels DAC, Hill PWS, Westermann AJ, Fisher RA, Thurston TL, Saliba A-E,
690 Blommestein I, Vogel J, Helaine S. 2018. Salmonella persisters undermine host
691 immune defenses during antibiotic treatment. Science 362:1156–1160.

692 39. Karamata D, Gross JD. 1970. Isolation and genetic analysis of temperature-
693 sensitive mutants of B. subtilis defective in DNA synthesis. Mol Gen Genet
694 108:277–287.

695 40. Rokop ME, Auchtung JM, Grossman AD. 2004. Control of DNA replication
696 initiation by recruitment of an essential initiation protein to the membrane of
697 Bacillus subtilis. Mol Microbiol 52:1757–1767.

698 41. Moriya S, Atlung T, Hansen FG, Yoshikawa H, Ogasawara N. 1992. Cloning of
699 an autonomously replicating sequence (ars) from the Bacillus subtilis
700 chromosome. Mol Microbiol 6:309–315.

701 42. Richter F, Fonfara I, Bouazza B, Schumacher CH, Bratovič M, Charpentier E,
702 Möglich A. 2016. Engineering of temperature- and light-switchable Cas9 variants.
703 Nucleic Acids Res 44:10003–10014.

704 43. Nihongaki Y, Kawano F, Nakajima T, Sato M. 2015. Photoactivatable CRISPR-
705 Cas9 for optogenetic genome editing. Nat Biotechnol 33:755–760.

706 44. Jain PK, Ramanan V, Schepers AG, Dalvie NS, Panda A, Fleming HE, Bhatia
707 SN. 2016. Development of Light-Activated CRISPR Using Guide RNAs with
708 Photocleavable Protectors. Angew Chem Int Ed Engl 55:12440–12444.

709 45. Richter F, Fonfara I, Gelfert R, Nack J, Charpentier E, Möglich A. 2017.
710 Switchable Cas9. Curr Opin Biotechnol 48:119–126.

711 46. Wenzel M, Müller A, Siemann-Herzberg M, Altenbuchner J. 2011. Self-inducible
712 Bacillus subtilis expression system for reliable and inexpensive protein production
713 by high-cell-density fermentation. Appl Environ Microbiol 77:6419–6425.

714 47. Guan C, Cui W, Cheng J, Zhou L, Guo J, Hu X, Xiao G, Zhou Z. 2015.
715 Construction and development of an auto-regulatory gene expression system in
716 Bacillus subtilis. Microb Cell Fact 14:150.

717 48. Tran DTM, Phan TTP, Doan TTN, Tran TL, Schumann W, Nguyen HD. 2020.
718 Integrative expression vectors with Pgrac promoters for inducer-free

719 overproduction of recombinant proteins in Bacillus subtilis. Biotechnol Rep (Amst)
720 28:e00540.

721 49. Wilson S, Garner E. 2021. An Exhaustive Multiple Knockout Approach to
722 Understanding Cell Wall Hydrolase Function in Bacillus subtilis. bioRxiv
723 2021.02.18.431929.

724 50. Livak KJ, Schmittgen TD. 2001. Analysis of relative gene expression data using
725 real-time quantitative PCR and the 2(-Delta Delta C(T)) Method. Methods
726 25:402–408.

727 51. Sauls JT, Cox SE, Do Q, Castillo V, Ghulam-Jelani Z, Jun S. 2019. Control of
728 Bacillus subtilis Replication Initiation during Physiological Transitions and
729 Perturbations. mBio 10.

730 52. Schindelin J, Arganda-Carreras I, Frise E, Kaynig V, Longair M, Pietzsch T,
731 Preibisch S, Rueden C, Saalfeld S, Schmid B, Tinevez J-Y, White DJ, Hartenstein
732 V, Eliceiri K, Tomancak P, Cardona A. 2012. Fiji: an open-source platform for
733 biological-image analysis. Nat Methods 9:676–682.

734 53. Berg S, Kutra D, Kroeger T, Straehle CN, Kausler BX, Haubold C, Schiegg M,
735 Ales J, Beier T, Rudy M, Eren K, Cervantes JI, Xu B, Beuttenmueller F, Wolny A,
736 Zhang C, Koethe U, Hamprecht FA, Kreshuk A. 2019. ilastik: interactive machine
737 learning for (bio)image analysis. Nat Methods 16:1226–1232.

738 54. Ducret A, Quardokus EM, Brun YV. 2016. MicrobeJ, a tool for high throughput
739 bacterial cell detection and quantitative analysis. Nat Microbiol 1:16077.

740 55. Engler C, Kandzia R, Marillonnet S. 2008. A one pot, one step, precision cloning
741 method with high throughput capability. PLoS One 3:e3647.

742 56. Schäfer H, Beckert B, Frese CK, Steinchen W, Nuss AM, Beckstette M, Hantke
743 I, Driller K, Sudzinová P, Krásný L, Kaever V, Dersch P, Bange G, Wilson DN,
744 Turgay K. 2020. The alarmones (p)ppGpp are part of the heat shock response of
745 Bacillus subtilis. PLoS Genet 16:e1008275.

746 57. Sherman BT, Hao M, Qiu J, Jiao X, Baseler MW, Lane HC, Imamichi T, Chang
747 W. 2022. DAVID: a web server for functional enrichment analysis and functional
748 annotation of gene lists (2021 update). Nucleic Acids Res gkac194.

749 58. Huang DW, Sherman BT, Lempicki RA. 2009. Systematic and integrative analysis
750 of large gene lists using DAVID bioinformatics resources. Nat Protoc 4:44–57.

751 59. Pedreira T, Elfmann C, Stülke J. 2022. The current state of SubtiWiki, the
752 database for the model organism Bacillus subtilis. Nucleic Acids Res 50:D875–
753 D882.

754 60. Perez-Riverol Y, Csordas A, Bai J, Bernal-Llinares M, Hewapathirana S, Kundu
755 DJ, Inuganti A, Griss J, Mayer G, Eisenacher M, Pérez E, Uszkoreit J, Pfeuffer J,
756 Sachsenberg T, Yilmaz S, Tiwary S, Cox J, Audain E, Walzer M, Jarnuczak AF,
757 Ternent T, Brazma A, Vizcaíno JA. 2019. The PRIDE database and related tools
758 and resources in 2019: improving support for quantification data. Nucleic Acids
759 Res 47:D442–D450.

760